

Computational Modeling of Microstructure Evolution in Solidification of Aluminum Alloys

M.F. ZHU, C.P. HONG, D.M. STEFANESCU, and Y.A. CHANG

In this article, a front tracking (FT) model and a modified cellular automaton (MCA) model are presented and their capabilities in modeling the microstructure evolution during solidification of aluminum alloys are demonstrated. The FT model is first validated by comparison with the predictions of the Lipton–Glicksman–Kurz (LGK) model. Calculations of the steady-state dendritic tip growth velocity and equilibrium liquid composition as a function of melt undercooling for an Al-4 wt pct Cu alloy exhibit good agreement between the FT simulations and the LGK predictions. The FT model is also used to simulate the secondary dendrite arm spacing as a function of local solidification time. The simulated results agree well with the experimental data. The MCA model is applied to simulate dendritic and nondendritic microstructure evolution in semisolid processing of an Al-Si alloy. The effect of fluid flow on dendritic growth is also examined. The solute profiles in equiaxed dendritic solidification of a ternary aluminum alloy are simulated as a function of cooling rate and compared with the prediction of the Scheil model. The MCA model is extended to the multiphase system for the simulation of eutectic solidification. A particular emphasis is made on the quantitative aspects of simulations.

I. INTRODUCTION

SOLIDIFICATION microstructure features can persist through subsequent processing and significantly affect the properties of the finished components. Control of solidification microstructures is thus very important in modern casting technology. To achieve the desired microstructures and hence to obtain high quality castings, it is of particular importance to understand the mechanisms of microstructure formation. However, solidification is a complicated process controlled by the interplay of thermal, solutal, capillary, thermodynamics, and kinetics at a variety of length and time scales. To better understand the underlying physics in this process, a complete temporal description of microstructure evolution becomes crucial. For this purpose, there is a considerable potential for applying numerical simulation to provide satisfactory information on the interactions between transport phenomena and phase transition during solidification. Over the last decade, computational modeling, which enables extensive use of mathematics for solving complicated problems, has emerged as a powerful and important tool in studies of microstructural evolution in

various solidification processes. The significant advances in numerical techniques have made it possible to analyze transport phenomena, including heat, mass, and fluid flow in the mushy zone during solidification to a high level of detail. This leads to the development of various deterministic and stochastic models for the simulation of microstructure evolution during solidification.^[1,2] The models based on the cellular automaton (CA) technique can reproduce most of the dendritic features observed experimentally with an acceptable computational efficiency. They have also demonstrated a potential for practical application. As a result, CA models have recently drawn great interest in academia and achieved considerable advances in modeling of a range of phase transitions during solidification at meso- and microscales.

Following the earlier attempts of Hesselbarth *et al.*^[3] and Brown *et al.*,^[4] Rappaz and Gandin developed a mesoscale CA model for the prediction of solidification grain structures.^[5] Their model includes the detailed physics of nucleation, growth kinetics, and crystallographic orientation. The model can simulate the time-dependent grain structure evolution, in which the individual grains are identified and their shapes and sizes can be shown graphically. Thereafter, a series of studies have been reported by Rappaz's group,^[6–9] Hong's group,^[10,11,12] and other researchers^[13,14] on simulation of grain structures formed in various casting processes. Taking into account the effect of convection, CA models were able to simulate the deflection behavior of the columnar grains solidified in a flowing melt^[15] or in the twin-roll strip casting process.^[16]

It should be noted that the dendrite growth velocity in the mesoscale CA models mentioned previously is related only to the local temperature in the solidifying region. Thus, the individual grains do not interact directly until they touch each other. Therefore, these models are unable to describe more detailed features such as side branching and the formation of second phases (eutectic). This limitation was first overcome by Dilthey and Pavlik^[17] in 1998. They developed a modified CA model in which the local velocity of

M.F. ZHU, Professor, is with the School of Materials Science and Engineering, Southeast University, Nanjing 210096, P.R. China. Contact e-mail: zhurf@seu.edu.cn. C.P. HONG, Professor and Director of the Center for Computer-Aided Materials Processing (CAMP), is with the Department of Metallurgical Engineering, Yonsei University, Seoul 120-749, Korea. D.M. STEFANESCU, FEF Key Professor, is with the Department of Materials Science and Engineering, The Ohio State University, Columbus, OH 43210. Y.A. CHANG, Wisconsin Distinguished Professor, is with the Department of Materials Science and Engineering, University of Wisconsin-Madison, Madison, WI 53706.

This article is based on a presentation made in the symposium "Simulation of Aluminum Shape Casting Processing: From Design to Mechanical Properties," which occurred March 12–16, 2006, during the TMS Spring Meeting in San Antonio, Texas, under the auspices of the Computational Materials Science and Engineering Committee, the Process Modeling, Analysis and Control Committee, the Solidification Committee, the Mechanical Behavior of Materials Committee, and the Light Metal Division/Aluminum Committee.

the solid/liquid (SL) interface is calculated from the complete solution of the transport equations for the solid and liquid phases including the boundary condition of solute balance at the moving SL interface. The model was successfully applied to simulation of the dendritic features formed in welding and thus the length scale of the CA method was extended from mesoscale to microscale. Thereafter, Nastac^[18] further modified the model by incorporating the time-dependent solution of the heat transport equation enabling the simulation of constrained and unconstrained growth and of the columnar-to-equiaxed transition (CET). Based on a similar methodology of the complete solution of the transport equations, Lee and co-workers^[19,20] developed a CA-FD model, which was able to simulate the dendrites with various orientations by using a modified decentered-square growth algorithm. In 2001, two of the present authors (Zhu and Hong) developed a modified CA (MCA) model by extending a previous mesoscale CA model. The model has been applied to simulate two-dimensional (2-D) and three-dimensional (3-D) single or multidendritic growth,^[21,22] nondendritic or globular microstructure evolution in the semisolid process,^[23] the dendritic growth with melt convection,^[24,25] and the microstructure formation in regular and irregular eutectic alloys.^[26,27] Recently, Zhu *et al.* extended the model to the ternary alloy system by coupling it with the thermodynamic and phase equilibrium calculation engine PanEngine.^[28]

Considering that most CA approaches mentioned previously can only give qualitative graphical outputs and have less quantitative capabilities, Beltran-Sanchez and Stefanescu (BSS)^[29,30] developed a model based on the CA concepts but using virtual tracking of the sharp SL interface for simulation of solutal dendrite growth in the low Péclet regime. The most important novel aspect of the model is a solution proposed to eliminate the mesh anisotropy and mesh dependency of CA calculations. The solution includes new methods for calculation of the SL interface curvature, normal velocity, and trapping rules for new interface cells. The quantitative capabilities of the model are well demonstrated by validation of the simulation results with experimental data and the classic Lipton–Glicksman–Kurz (LGK) theory. Based on the previous efforts, more recently, two of the present authors (Zhu and Stefanescu) developed a front tracking (FT) model for the simulation of dendrite growth in the low Péclet number regime.^[31] The model not only has the quantitative capabilities for the predictions of dendrite growth in solidification of alloys, but also is able to reproduce very realistic growth features for both equiaxed and columnar dendrites. This article briefly describes the MCA model and the derived FT model and presents some applications of both models in modeling of microstructure evolution of aluminum alloys in various solidification processes.

II. MODEL DESCRIPTION AND NUMERICAL METHOD

The MCA model was developed by extending a mesoscale CA model^[5,6] to include the effect of constitutional undercooling and curvature undercooling on the equilibrium interface temperature. The velocity of the moving SL interface is calculated from the analytical theories of

dendrite growth or by introducing a kinetics coefficient. The details of the growth algorithms for 2-D and 3-D dendrite simulation and 2-D eutectic simulation of the MCA model can be found elsewhere.^[21–27] On the other hand, the derived FT model calculates the evolution of the SL interface directly from the difference between the local equilibrium composition and the local actual liquid composition. This allows the simulations of dendrite growth without the need of a kinetic parameter and it can accurately describe the dynamics of dendrite growth from the initial unstable stage to the steady-state stage. The governing equations and numerical algorithms for calculating the temperature field, the solute field, the interface curvature, the crystallographic anisotropy, and the kinetics of dendritic growth are described subsequently.

The governing equation for transient heat conduction is given by

$$\rho C_p \frac{\partial T}{\partial t} = \nabla \cdot (\lambda \nabla T) + \rho \Delta H \frac{\partial f_s}{\partial t} \quad [1]$$

where T is temperature, t is time, ρ is density, C_p is specific heat, f_s is the solid fraction, λ is thermal conductivity, and ΔH is latent heat of solidification.

As the dendrite grows, the growing cells reject solute at the SL interface. Solute partition between liquid and solid at the SL interface is considered according to $C_s = kC_l$. Solute diffusion within the entire domain is then calculated with

$$\frac{\partial C}{\partial t} = \nabla \cdot (D \nabla C) + C(1 - k) \frac{\partial f_s}{\partial t} \quad [2]$$

where C is composition, D is the solute diffusion coefficient, and k is the solute partition coefficient. The second term on the right-hand side denotes the amount of solute rejected at the SL interface.

Note that the local interface equilibrium composition of a crystal residing in an undercooled liquid is higher than the local actual liquid composition. To reach the equilibrium composition, solidification begins. As the dendrite grows, latent heat and solute are released at the SL interface, which results in a thermal and a solutal gradient ahead of the interface, leading to heat and mass transport in the domain. The dendrite growth also changes the interface curvature. The new thermal field and interface curvature generate new interface equilibrium composition. The mass transfer also results in a new solute field, which determines the local actual interface liquid composition. This interaction between heat/mass transport and dendritic growth continues to the end of solidification. Accordingly, in the FT model, the driving force for dendritic growth is considered to be controlled by the difference between local interface equilibrium composition and local actual liquid composition. Based on the thermodynamic concept of the local equilibrium between liquid and solid phases, the interface equilibrium composition C_l^* can be calculated with

$$C_l^* = C_0 + \frac{T^* - T_l^{eq}}{m_l} + \frac{\Gamma K f(\varphi, \theta_0)}{m_l} \quad [3]$$

where T^* is the interface temperature; T_l^{eq} is the equilibrium liquidus temperature at the initial composition C_0 ; m_l is the liquidus slope; Γ is the Gibbs–Thomson coefficient;

K is the interface curvature; and $f(\varphi, \theta_0)$ is a function accounting for the anisotropy of the surface tension, in which θ_0 indicates the crystallographic orientation. The calculated local interface equilibrium composition C_l^* is then compared with the local actual liquid composition C_l determined by solving Eq. [2]. If the difference $\Delta C = C_l^* - C_l > 0$, the solid fraction of this cell will increase. According to the equilibrium condition at the SL interface, during one time-step interval Δt , the increase in solid fraction Δf_s of an interface cell can be evaluated by

$$\Delta f_s = (C_l^* - C_l) / (C_l^* (1 - k)) \quad [4]$$

When the sum of solid fraction in an interface cell equals one, the state of this interface cell is assigned as solid. At the end of a time-step, the solid fraction field is scanned and new interface cells are captured using a virtual interface tracking scheme proposed by BSS.^[30]

The local interface curvature K and the anisotropy of surface tension $f(\varphi, \theta_0)$ in Eq. [3] are calculated using the following equations:

$$K = \left[\left(\frac{\partial f_s}{\partial x} \right)^2 + \left(\frac{\partial f_s}{\partial y} \right)^2 \right]^{-3/2} \times \left[2 \frac{\partial f_s}{\partial x} \frac{\partial f_s}{\partial y} \frac{\partial^2 f_s}{\partial x \partial y} - \left(\frac{\partial f_s}{\partial x} \right)^2 \frac{\partial^2 f_s}{\partial y^2} - \left(\frac{\partial f_s}{\partial y} \right)^2 \frac{\partial^2 f_s}{\partial x^2} \right] \quad [5]$$

$$f(\varphi, \theta_0) = 1 - \delta \cos [4(\varphi - \theta_0)] \quad [6]$$

$$\varphi = \cos^{-1} \left[\frac{\partial f_s / \partial x}{((\partial f_s / \partial x)^2 + (\partial f_s / \partial y)^2)^{1/2}} \right] \quad [7]$$

where δ is the anisotropy coefficient.

III. RESULTS AND DISCUSSION

A. Comparison of the FT Model to the LGK Prediction for an Al-4 Wt Pct Cu Alloy

To validate the quantitative capabilities of the FT model, the simulated steady-state growth features of an Al-4 pct Cu alloy as a function of melt undercooling were compared with the predictions of the Lipton–Glicksman–Kurz (LGK) model.^[32] At the beginning of the simulation, a solid seed of composition kC_0 with a crystallographic orientation of 0 deg with respect to the horizontal direction was placed at the center of the domain. Other cells in the domain were filled with the undercooled liquid with an assigned initial composition and temperature. During the dendrite growth, the rejected latent heat was extracted from the four boundary walls to keep the heat balance in the domain. Because there exists an initial transient period over which the dendrite growth reaches steady state and it is of the order of D_l/V_n^2 , where V_n is the steady-state tip velocity,^[1,30] the steady-state tip parameters were measured after two times of this transient period. Figure 1 presents the comparison of steady-state tip growth velocity and equilibrium composition for an Al-4 wt pct Cu alloy with various melt undercoolings.

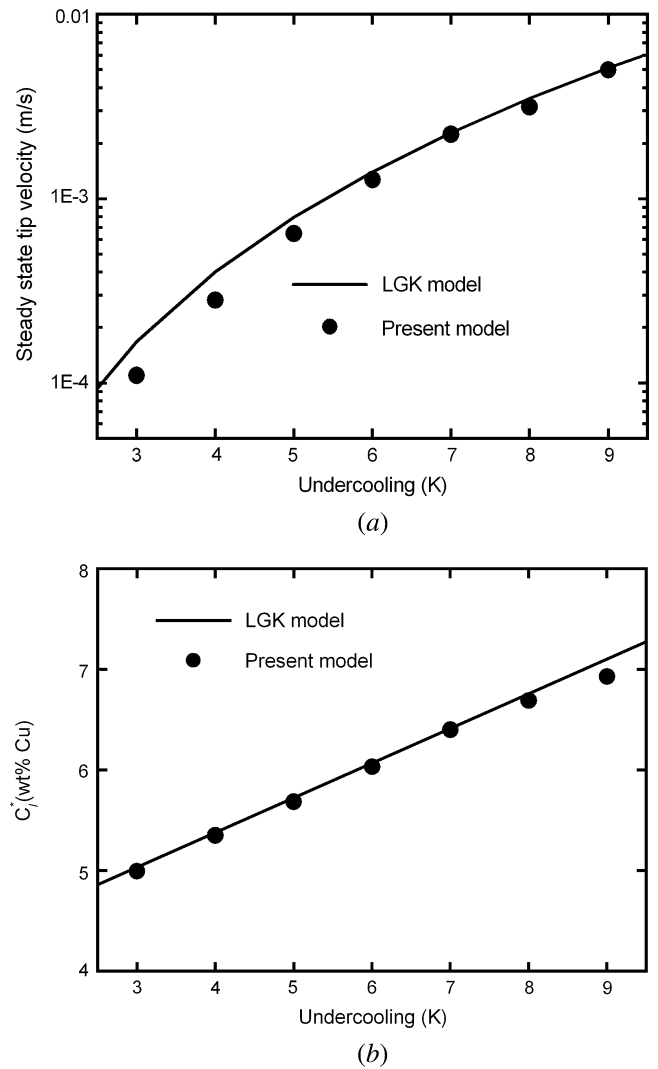


Fig.1—Comparison of simulations to the LGK predictions for an Al-4 wt pct Cu alloy: (a) the steady-state tip velocity and (b) the equilibrium liquid composition at the steady-state tip.

It can be noted that the agreement between the FT simulations and the LGK predictions appears to be very good.

B. Prediction of Secondary Dendrite Arm Spacing

Secondary dendrite arm spacing (SDAS) has been known to be mainly dependent on the local solidification time. The simulations were carried out for an Al-4.5 wt pct Cu alloy using the FT model. The temperature in the entire domain was assumed to be uniform and cooled from the liquidus temperature with a constant cooling rate. Figure 2 illustrates the evolution of SDAS simulated by the FT mode with a cooling rate of 10 °C/s. It is noted that the competitive growth of secondary dendrite arms occurs at the initial stage, followed by coarsening of the selected arms. Figure 3 presents the simulated and experimental variation of SDAS with local solidification time. It can be seen that the simulated values of SDAS that increase with the local solidification time coincide well with the experimental data.^[33]

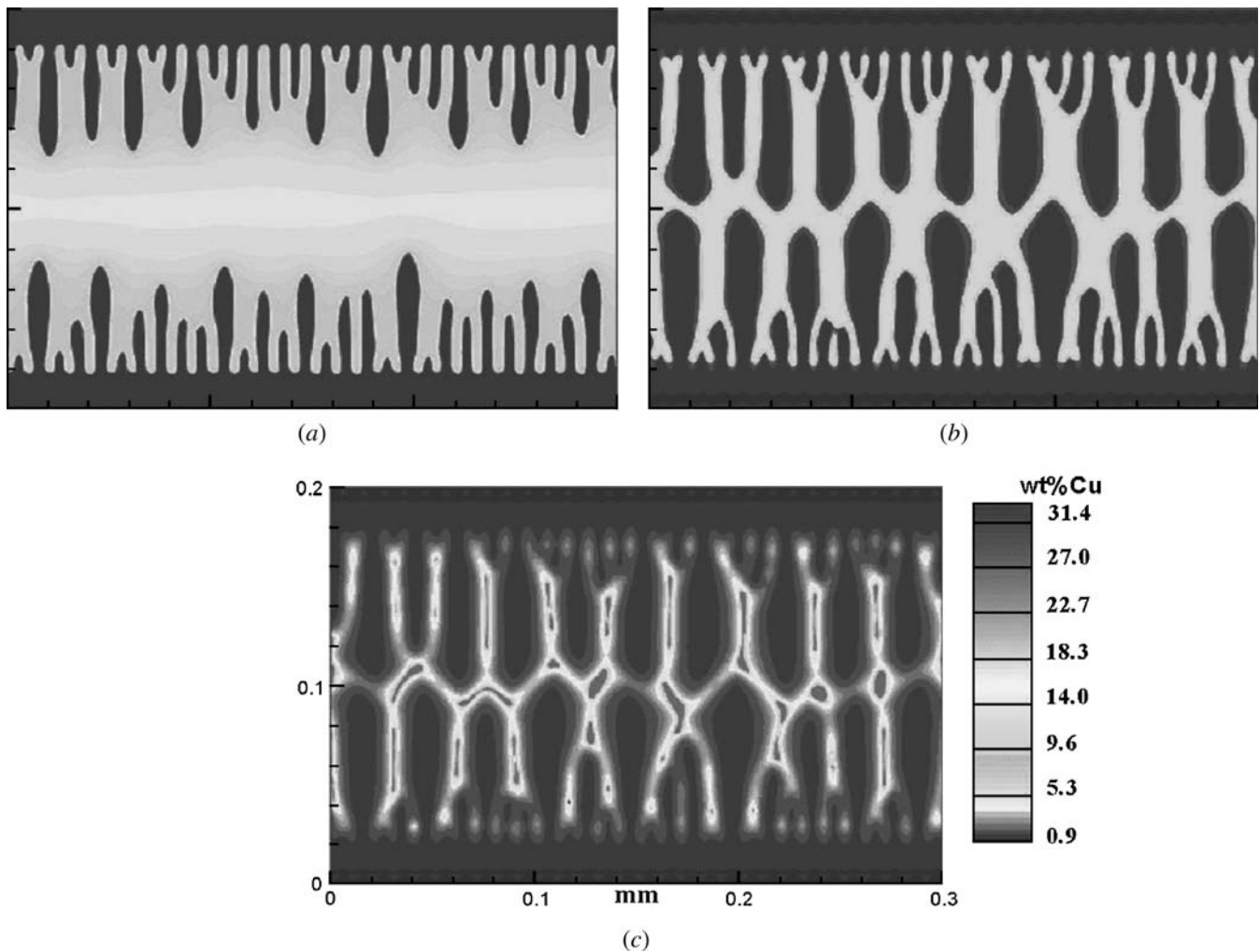


Fig. 2—Simulated evolution of the secondary dendrite arms for an Al-4.5 wt pct Cu alloy with a cooling rate of $10\text{ }^{\circ}\text{C/s}$ ($\Delta x = 1\text{ }\mu\text{m}$): (a) 0.8 s, (b) 1.67 s, and (c) 10 s.

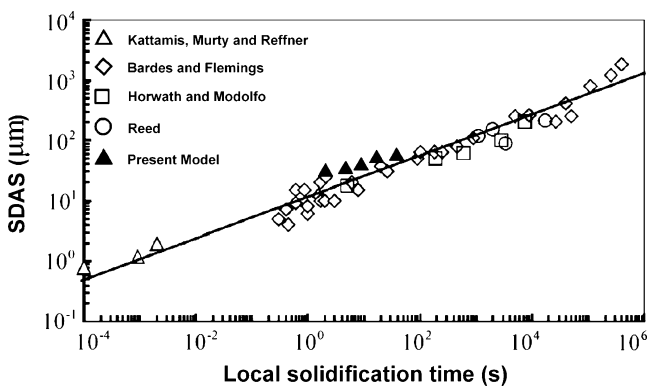


Fig. 3—Comparison of SDAS with local solidification times between simulations and literature data^[33] for an Al-4.5 wt pct Cu alloy.

C. Simulation of Dendritic and Nondendritic Microstructures

In recent years, semisolid casting processes have drawn great interest among casting manufacturers. This technology needs to produce a special feeding material with nondendritic or globular microstructures. Figure 4 presents a

simulated microstructure map for an Al-7 wt pct Si alloy obtained from different nucleation densities and solidification cooling rates.^[34] In the figure, N indicates the relative density of nuclei in the melt. When $n = 1$ with a cooling rate of $0.2\text{ }^{\circ}\text{C/s}$, a globular microstructure with grain size of $120\text{ }\mu\text{m}$ can be obtained. If N increases 15 times, the grain size is decreased to around 40 to $50\text{ }\mu\text{m}$. Similarly, when N increases 1000 times, we can obtain a very fine globular microstructure with a grain size of about $10\text{ }\mu\text{m}$. In addition, our previous simulation studies show that uniform distribution of nuclei will also be favorable for the formation of globular structure.^[23] Based on these simulations, an advanced rheocasting process, called “H-NCM (Hong Nanocasting Method)”^[34] was developed. Figure 5 shows the microstructures of A356 alloy obtained by various semisolid casting processes, such as a conventional thixo-casting,^[35] a conventional rheocasting,^[36] and H-NCM.^[37,38] As can be seen, the globular microstructure obtained by H-NCM is much finer than those of other methods.

D. Simulation of Dendritic Growth with Melt Convection

Flow of molten metal in solidification processes conducted under a gravitational field is an unavoidable

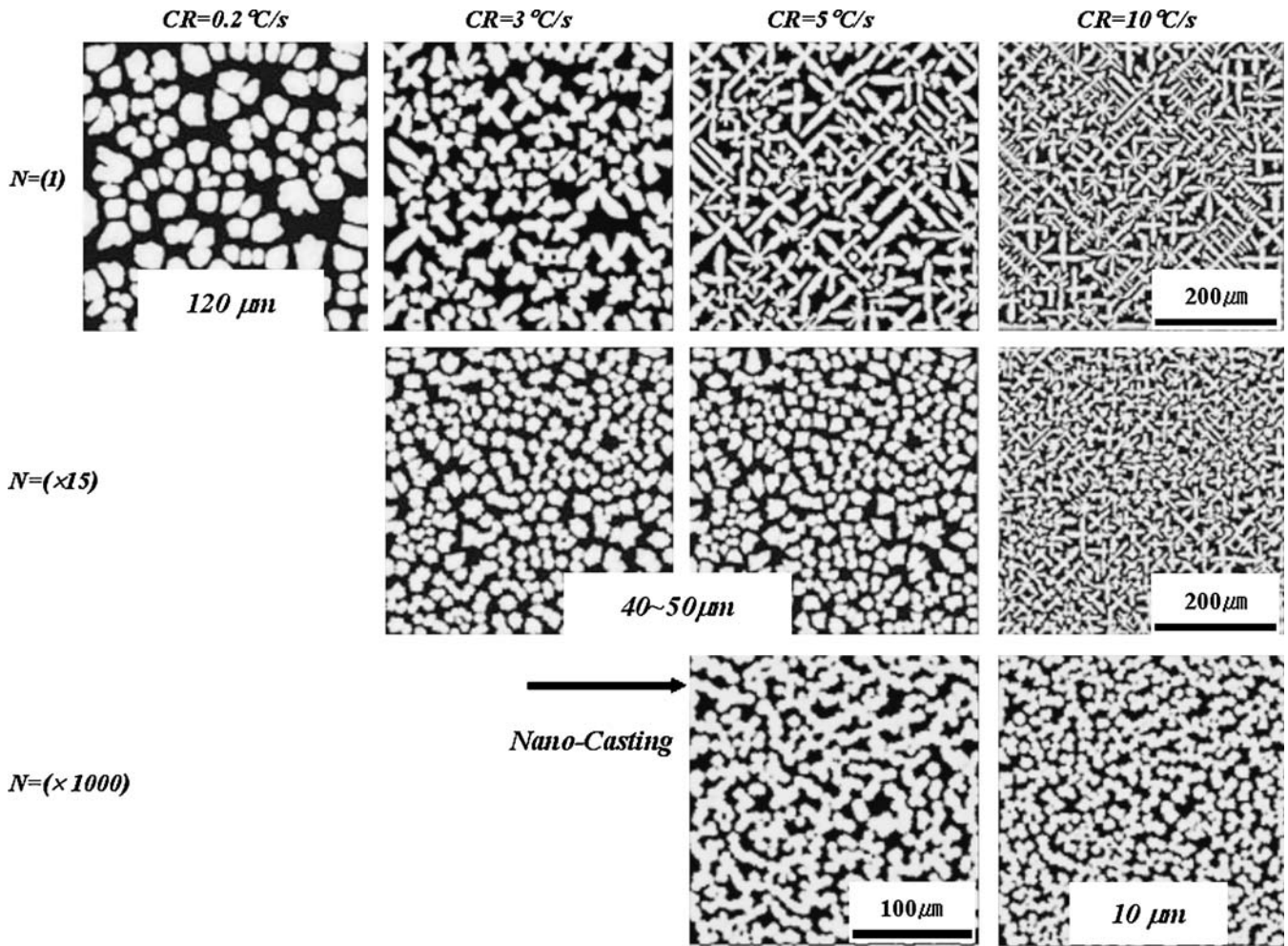


Fig. 4—A simulated microstructure map with various nucleation densities and cooling rates.^[34]

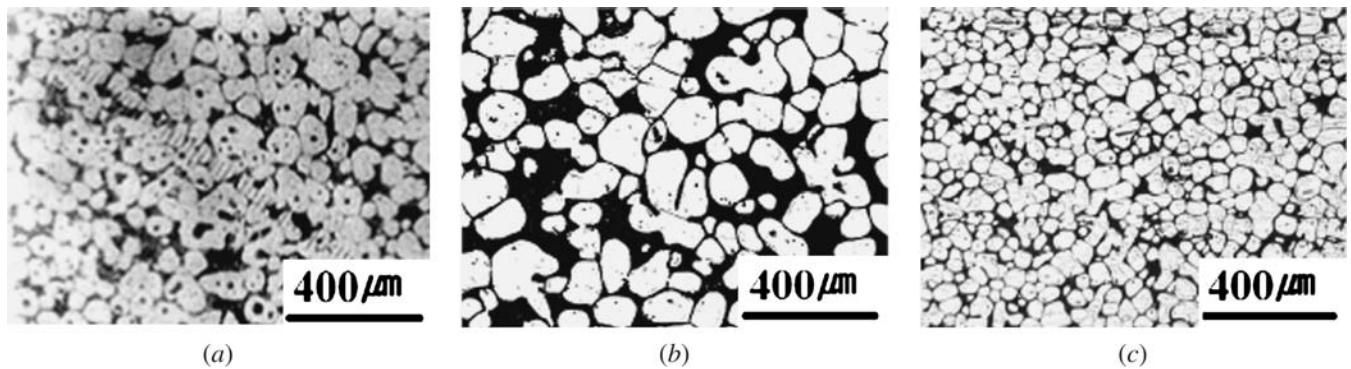


Fig. 5—Comparison of globular microstructures of A356 alloy obtained by (a) conventional thixocasting,^[35] (b) conventional rheocasting,^[36] and (c) H-NCM.^[37,38]

phenomenon, either because of natural buoyancy or forced convection. Since melt convection alters the local heat and solutal transfer at the SL interface, the microstructure is strongly affected by the presence of flow. Thus, to understand the effect of convection on microstructural development is important for controlling microstructures. The MCA coupled with a transport model was applied to simulate the dendritic growth in a flowing melt.^[24,25] In this case, the solute field is controlled by both diffusion and

convection. Figure 6 shows the simulated dendritic features of directionally solidified Al-2 wt pct Cu alloy with or without flow. The calculation domain consists of 240×200 cells with a cell size of $2.5 \mu\text{m}$. The temperature field in the entire domain was assumed to be homogeneous with an undercooling of $10 \text{ }^\circ\text{C}$. At the beginning of calculation, six solid seeds having a crystallographic orientation of 0 deg with respect to the vertical direction were assigned at the bottom of the domain. It can be seen that in the case

of no melt flow, a symmetrical dendritic morphology is produced. However, the dendrites solidified with melt flow exhibit an asymmetrical growth morphology. Side branches are largely favored on the lead edge of the main stem and nearly completely suppressed on the other side. Note that fluid flow significantly distorts the solute profile around the growing dendrites. The solute concentration is lower in the liquid around the forehead of the dendrites and higher on the rear of the main stem, which represses the side branching into the secondary dendrite arms on the right hand of dendrites due to solute undercooling. Another interesting phenomenon is that the main stems are no longer vertical and obviously deflected into the incoming flow.

E. Simulation of Microstructure and Microsegregation in a Ternary Aluminum Alloy

Most commercial aluminum alloys are multicomponent systems. The MCA model has been coupled with the thermodynamic and phase equilibrium calculation engine PanEngine to simulate the microstructures and microsegregation in a ternary aluminum alloy.^[28] In the model, the dendrite growth is considered to be driven by the difference between the local equilibrium liquidus temperature and the local actual temperature, incorporating the effect of curva-

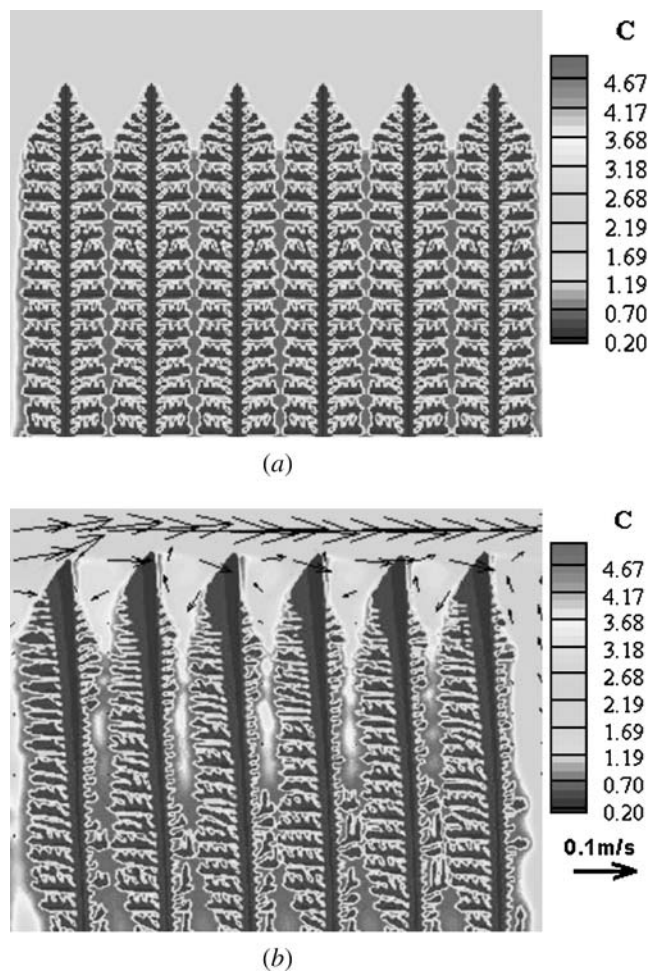


Fig. 6—Simulated dendrite morphology of an Al-2 wt pct Cu alloy under directional solidification with an undercooling of 10 °C: (a) without flow and (b) with flow ($U_{in} = 0.015$ m/s).

ture. Based on the interface liquid compositions of two solutes, which are determined by numerically solving the mass transport equation in the entire domain, the local equilibrium temperature and the solid compositions of two solutes are calculated with the aid of PanEngine. Figure 7 shows the simulated dendrite morphology and the composition maps of an Al-3.9 wt pct Cu-0.9 wt pct Mg alloy with a cooling rate of 15 °C/s. It can be seen that the central region of the dendrites exhibits lower contents than the outside shell for both Cu and Mg solutes. The variation of solid compositions with the increase of solid fraction was recorded for comparison with the predictions of the Scheil model. It is known that the Scheil model is derived based on the assumptions of no diffusion in solid and complete mixing in liquid. To analyze the effect of diffusion in liquid on the microsegregation, zero solid diffusivity and finite liquid diffusivity were adopted for the simulations.

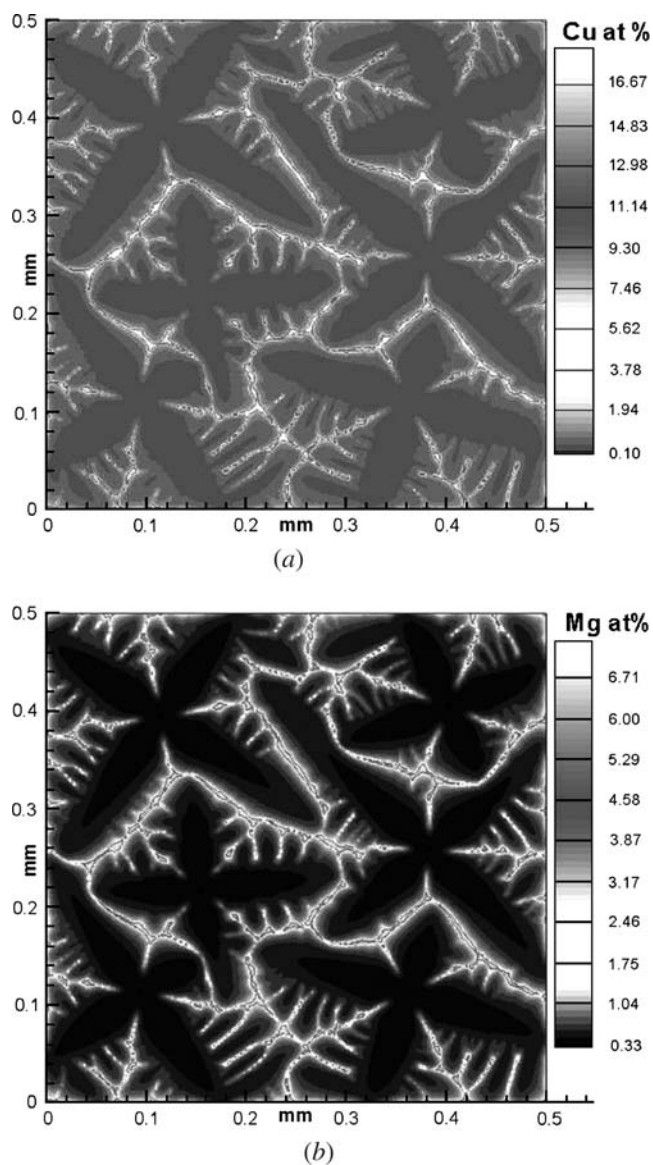


Fig. 7—Simulated equiaxed dendrite morphology and solute fields of (a) Cu and (b) Mg for an Al-3.9 wt pct Cu-0.9 wt pct Mg alloy solidified with 15 °C/s (domain: 250×250 meshes with $\Delta x = 2 \mu\text{m}$).

The simulated solid composition profiles of two solutes with the cooling rates of 0.1 °C/s, 15 °C/s, and 100 °C/s are compared with the Scheil predictions in Figure 8. Note

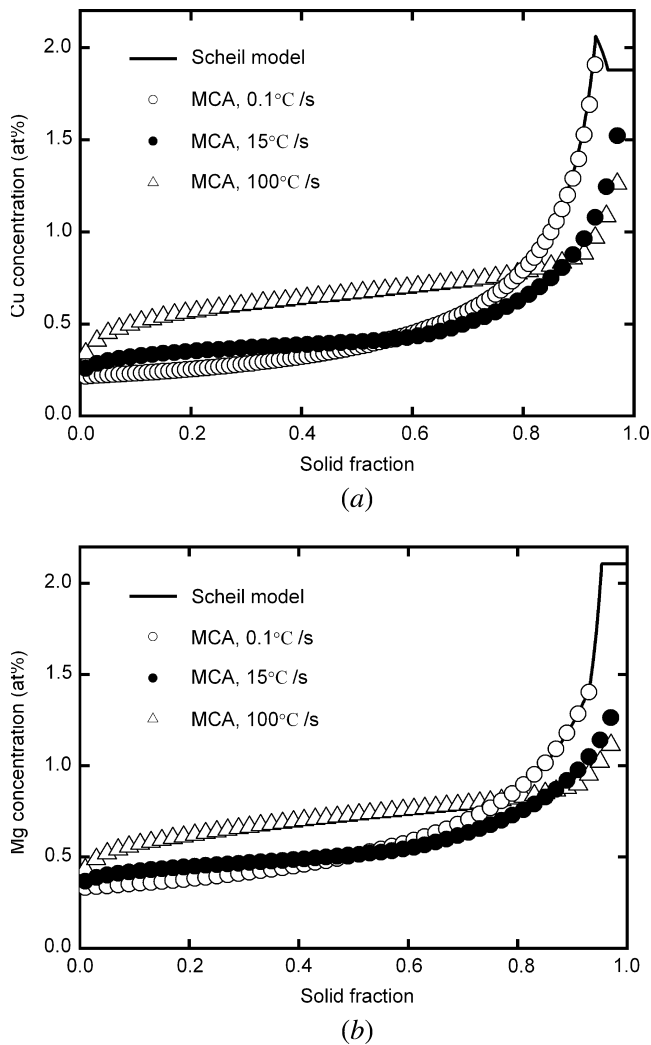


Fig. 8—Comparison between the Scheil model and the MCA model for predicting solute concentration profiles of (a) Cu and (b) Mg as a function of solid fraction for an Al-3.9 wt pct Cu-0.9 wt pct Mg alloy.

that the solid compositions of both solutes Cu and Mg predicted by the Scheil model are relatively lower in the early solidification stage but higher in the later stage compared with the simulated profiles. This is due to the fact that the Scheil prediction was obtained assuming complete mixing in the liquid, whereas the simulations involved the limited liquid diffusivity using the realistic liquid diffusion coefficients. With increasing solidification rate, the extent of the inhomogeneous solute distribution in liquid increases. Consequently, it is understandable that the difference between the simulated data and the Scheil profiles increases with the solidification rate. In the case of a very low cooling rate of 0.1 °C/s, the calculated data are nearly superimposed on the Scheil profiles. In our previous work^[28] we also performed the simulations with both realistic solid and liquid diffusivities and compared the simulation results with experimental data for a cooling rate of 0.23 °C/s. The composition profile with nonzero solid diffusivity is higher in the early stage but lower later than that obtained with zero solid diffusivity, indicating the effect of back diffusion. Regarding the comparison with the experiment, the simulated data are mostly found below the experimental data. Nevertheless, they exhibit the same tendency of the solute compositions increasing with solid fraction. Possible reasons attributed to the discrepancies between the simulation results and the experimental data were analyzed in Reference 28.

F. Simulation of Eutectic Microstructure

In the most widely used cast aluminum alloys, the typical microstructure consists of primary dendrites and interdendritic eutectics. The MCA model has been extended to a multiphase system, including liquid and two solid phases, for the simulation of eutectic microstructures.^[26,27] Figure 9 shows a microstructure evolution simulated with an Al-7 wt pct Si alloy. The simulation started from the liquidus temperature with a constant cooling rate of 1 °C/s. When the temperature reached the eutectic temperature, the remaining liquid underwent an isothermal eutectic transformation. In Figure 9, the primary dendrites were simulated using the FT model, while the eutectics were simulated using the multiphase MCA model. It can be noted from Figure 9(b)

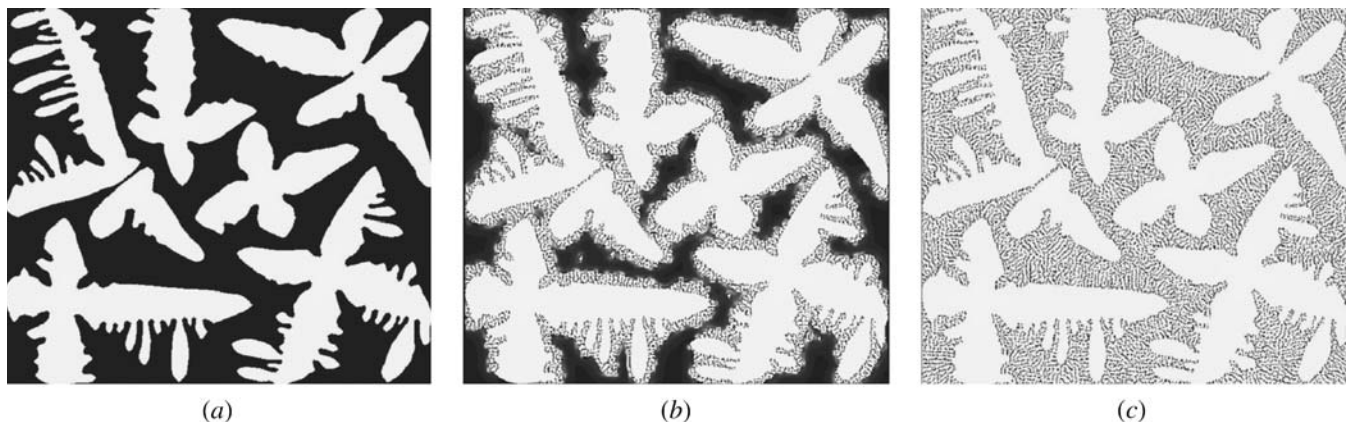


Fig. 9—Simulated evolution of the microstructure of an Al-7 wt pct Si alloy: (a) primary dendrite formation, (b) isothermal eutectic transformation, and (c) the microstructure at the end of solidification (domain: 600 × 530 meshes with $\Delta x = 1 \mu\text{m}$).

that the nucleation and growth of eutectics are mostly based on the primary dendrites.

IV. CONCLUSIONS

A modified CA model and a front tracking model have been developed and applied to simulate the evolution of solidification microstructure and solute distribution during solidification of aluminum alloys. The quantitative capabilities of the models were demonstrated by analytical and experimental validation. The models are able to represent a wide range of realistic growth phenomena both for the formation of primary phase, including dendritic and globular microstructure, and for the eutectic growth. The simulations offer insight into the phenomenon of microstructure evolution under various conditions and also provide information for understanding the physics of solidification of alloys. This will play an important role in alloy design and process development for industrial applications. Efforts will be continuously devoted to further improving the models concerned with remelting and coarsening of phases, as well as the formation of multiphase microstructures evolving in successive steps along with the solidification path in multicomponent alloys.

ACKNOWLEDGMENTS

The authors thank Dr. Qigui Wang, GM–Powertrain Engineering HQ, for his kind comments on this article. The research of MFZ was supported by NSFC under Grant Nos. 50371015 and 50471030. YAC thanks the NSF through FRG Grant No. DMR-0309468 and the Wisconsin Distinguished Professorship for support.

REFERENCES

1. W.J. Boettinger, S.R. Coriell, A.L. Greer, A. Karma, W. Kurz, M. Rappaz, and R. Trivedi: *Acta Mater.*, 2000, vol. 48, pp. 43-70.
2. D.M. Stefanescu: *Iron Steel Inst. Jpn. Int.*, 1995, vol. 35, pp. 637-50.
3. H.W. Hesselbarth and I.R. Gobel: *Acta Mater.*, 1991, vol. 39, pp. 2135-43.
4. S.G. Brown and J.A. Spittle: *Scripta Metall.*, 1992, vol. 27, pp. 1599-1603.
5. M. Rappaz and C.-A. Gandin: *Acta Metall. Mater.*, 1993, vol. 41, pp. 345-60.
6. C.-A. Gandin and M. Rappaz: *Acta Metall. Mater.*, 1994, vol. 42, pp. 2233-46.
7. M. Rappaz, Ch.-A. Gandin, J.-L. Desbiolles, and Ph. Thevos: *Metall. Mater. Trans. A*, 1996, vol. 27A, pp. 695-705.
8. C.-A. Gandin and M. Rappaz: *Acta Mater.*, 1997, vol. 45, pp. 2187-95.
9. C.-A. Gandin, Ch.-A. Gandin, J.-L. Desbiolles, and Ph. Thevos: *Metall. Mater. Trans. A*, 1999, vol. 30A, pp. 3153-65.
10. K.Y. Lee and C.P. Hong: *Iron Steel Inst. Jpn. Int.*, 1997, vol. 37, pp. 38-46.
11. I.S. Cho and C.P. Hong: *Iron Steel Inst. Jpn. Int.*, 1997, vol. 37, pp. 1098-1106.
12. Y.H. Chang, S.M. Lee, K.Y. Lee, and C.P. Hong: *Iron Steel Inst. Jpn. Int.*, 1998, vol. 38, pp. 63-70.
13. L. Nastac: *JOM*, 1998, vol. 50(3), pp. 30-35.
14. K. Ravindran, S.G.R. Brown, and J.A. Spittle: *Mater. Sci. Eng., A*, 1999, vol. 269, pp. 90-97.
15. S.Y. Lee, S.M. Lee, and C.P. Hong: *Iron Steel Inst. Jpn. Int.*, 2000, vol. 40, pp. 48-57.
16. H. Takatani, C.-A. Gandin, and M. Rappaz: *Acta Mater.*, 2000, vol. 48, pp. 675-88.
17. U. Dilthey and V. Pavlik: in *Modeling of Casting, Welding and Advanced Solidification Processes VIII*, San Diego, CA, June 7-12, 1998, B.G. Thomas and C. Beckermann, eds., TMS, Warrendale, PA, 1998, pp. 589-96.
18. L. Nastac: *Acta Mater.*, 1999, vol. 47, pp. 4253-62.
19. W. Wang, P.D. Lee, and M. Mclean: *Acta Mater.*, 2003, vol. 51, pp. 2971-87.
20. H.B. Dong and P.D. Lee: *Acta Mater.*, 2005, vol. 53, pp. 659-68.
21. M.F. Zhu and C.P. Hong: *Iron Steel Inst. Jpn. Int.*, 2001, vol. 41, pp. 436-45.
22. M.F. Zhu and C.P. Hong: *Iron Steel Inst. Jpn. Int.*, 2002, vol. 42, pp. 520-26.
23. M.F. Zhu, J.M. Kim, and C.P. Hong: *Iron Steel Inst. Jpn. Int.*, 2001, vol. 41, pp. 992-98.
24. M.F. Zhu, S.Y. Lee, and C.P. Hong: *Phys. Rev. E*, 2004, vol. 69, p. 061610.
25. M.F. Zhu, T. Dai, S.Y. Lee, and C.P. Hong: *Sci. China Ser. E*, 2005, vol. 48 (3), pp. 241-57.
26. M.F. Zhu and C.P. Hong: *Phys. Rev. B: Condens. Matter Mater. Phys.*, 2002, vol. 66, p. 155428.
27. M.F. Zhu and C.P. Hong: *Metall. Mater. Trans. A*, 2004, vol. 35A, pp. 1555-63.
28. M.F. Zhu, W. Cao, S.-L. Chen, F.-Y. Xie, C.P. Hong, and Y.A. Chang: *Trans. Nonferrous Met. Soc. China*, 2006, in press.
29. L. Belteran-Sanchez and D.M. Stefanescu: *Metall. Mater. Trans. A*, 2003, vol. 34A, pp. 367-82.
30. L. Belteran-Sanchez and D.M. Stefanescu: *Metall. Mater. Trans. A*, 2004, vol. 35A, pp. 2471-85.
31. M.F. Zhu and D.M. Stefanescu: *Modeling of Casting, Welding and Advanced Solidification Processes XI*, Club Med, Opio, France, May 28-June 2, 2006, C.-A. Gandin, and M. Bellet, eds., TMS, Warrendale, PA, pp. 473-80.
32. J. Lipton, M.E. Glicksman, and W. Kurz: *Mater. Sci. Eng.*, 1984, vol. 65, pp. 57-63.
33. M.C. Flemings, T.Z. Kattamis, and B.P. Bardes: *AFS Trans.*, 1991, vol. 99, pp. 501-06.
34. K. Watanabe, M. Itamura, J.M. Kim, and C.P. Hong: *Die Mould Technol.*, 2005, vol. 20 (5), pp. 33-36.
35. M.C. Flemings and K.P. Young: *Rheocasting, Yearbook of Science and Technology*, McGraw-Hill, New York, NY, 1978.
36. UBE Industries Ltd.: European Patent No. EP0 745 694 A1, Dec. 1996.
37. C.P. Hong: JP Patent No. 3,549,054, 2003.
38. C.P. Hong: U.S. Patent No. 6,942,009 (2005).